Topological superconductivity in a two-dimensional Weyl SSH model

Peter Rosenberg [1] and Efstratios Manousakis [2,3]

[1]*Département de Physique and Institut Quantique, Université de Sherbrooke, Québec, Canada J1K 2R1*
[2]*National High Magnetic Field Laboratory and Department of Physics, Florida State University, Tallahassee, Florida 32306, USA*
[3]*Department of Physics, National and Kapodistrian University of Athens, Panepistimioupolis, Zografos, 157 84 Athens, Greece*

We study the emergence of topological superconductivity in a two-dimensional Weyl system, composed of stacked Su-Schrieffer-Heeger (SSH) chains. A previous analysis of the model showed that the addition of an attractive Hubbard interaction between spinful electrons leads to a superconducting state that has an intricate pairing structure, but is topologically trivial. Here we consider a pairing interaction that couples spinless fermions on opposite sublattices within the same unit cell. We observe that this physically motivated, momentum-independent pairing interaction induces a topological superconducting state, characterized by a gap function with a nontrivial phase, as well as Majorana and Fermi arc edge states along the edge perpendicular to the direction of the SSH dimerization. In addition, we observe a transition as a function of pairing interaction strength and chemical potential, indicated by a change in the sign of the topological charge carried by each of the four Bogoliubov-Weyl nodes.

I. INTRODUCTION

The discovery of topological materials marked the beginning of a new era in condensed matter physics, centered on the role of topology in condensed matter systems [1,2]. As the field has developed, many models have been constructed to describe these novel materials, but one of the earliest and most enduring is the Su-Schrieffer-Heeger (SSH) model [3]. The model, initially conceived to explain the emergence of solitons in quasi-one-dimensional materials such as polyacetylene, is based on a simple picture of one-dimensional chains with staggered hopping strengths [4]. Despite this apparent simplicity, the model has helped introduce various novel topological phenomena [5], including charge fractionalization, solitons, edge states, and topological transitions [4,6]. The model has also been emulated using cold atoms in optical lattices, where the Zak phase [5] has been measured [7] and the so-called Thouless charge pumping [8] has been realized as topological charge pumping [9–12].

Several variations of the SSH model have been developed and studied since its introduction, for instance models that include longer range hopping [13–15] or a two-leg ladder of SSH chains, known as the Creutz model [16,17], as well as other two-dimensional (2D) extensions [18]. In two previous publications, we studied superconductivity in a model consisting of an infinite array of SSH chains [19,20]. In particular, we focused on a parameter regime in which the normal state of the system is a Weyl semimetal.

The observation of superconductivity in topological materials, including Dirac and Weyl semimetals [21–24], has opened a rapidly evolving avenue of research in the field of topological condensed matter, with a focus on the interplay of superconductivity and topology. Topological superconduc-

tors, characterized by the presence of Majorana fermions, are believed to offer an ideal platform for quantum computing [25–29] and information, which has motivated a concentrated effort to characterize these states and discover their underlying mechanisms.

One well-studied class of topological superconductors comprises systems with momentum-dependent pairing interactions, for instance with p-wave or d-wave symmetry [30,31]. These systems are believed to support Majorana fermions with properties that make them well suited for applications in quantum computing [25,32]. Yet, it has proven difficult to discover or design materials with intrinsic p-wave pairing that might be used in quantum computing applications. In the context of cold atoms, proposals exist to generate p-wave superfluids from s-wave interactions [33]. Recent work on superconductivity in Weyl semimetals may, however, provide an alternative route towards real material realizations of topological superconductivity. These studies note that topological superconducting states can be induced in Weyl systems subject to conventional s-wave pairing interactions [34–36]. In the absence of interactions, these models describe Weyl systems characterized by a set of nodal points carrying topological charge. Upon the introduction of interactions, each node is split into a pair of Bogoliubov-Weyl nodes with zero-energy Majorana states at the boundaries.

Here we treat a lattice fermion model, which is a straightforward extension of the SSH model. The noninteracting component of the Hamiltonian describes a set of 1D SSH chains that are coupled via an interchain hopping term to form a 2D lattice. The model supports a Weyl semimetal state, with a single pair of nodes. The topological properties of this model, as well as its intricate pairing behavior in the presence
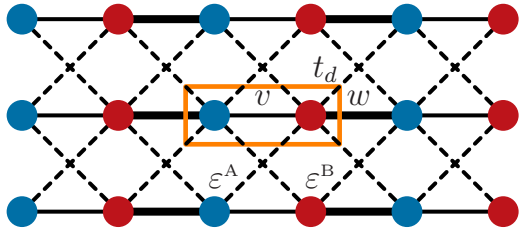
FIG. 1. Illustration of lattice with hopping terms. The unit cell is indicated by the orange box.

of an attractive Hubbard interaction, have been studied previously using a combined mean-field theory and auxiliary-field quantum Monte Carlo approach [19].

In the present work, we show that the presence of a momentum-independent interorbital pairing term coupling spinless fermions in the same unit cell yields a topological superconducting state with a gap function that has emergent p-wave character in the vicinity of the nodal points. This state is characterized by the presence of both zero-energy Majorana edge states and Bogoliubov-Weyl Fermi arc states. Our model provides a clear example of the emergence of topological superconductivity from a momentum-independent pairing term in a system with an underlying topological band structure, as well as an indication of the essential ingredients to realize topological superconducting states from momentum-independent interactions between bare particles.

II. MODEL

We consider the following lattice Hamiltonian:

$$\hat{H}_0 = -\sum_{n,m} v c_{n,m}^{(A)\dagger} c_{n,m}^{(B)} + w c_{n,m}^{(A)\dagger} c_{n-1,m}^{(B)} + \text{H.c.}$$

$$- \sum_{n,m} t_d c_{n,m}^{(B)\dagger} c_{n,m\pm 1}^{(A)} + t_d c_{n,m}^{(B)\dagger} c_{n+1,m\pm 1}^{(A)} + \text{H.c.}$$

$$+ \sum_{n,m,\alpha} (\varepsilon^\alpha - \mu) n_{n,m}^{(\alpha)}, \tag{1}$$

where the operator $c_{n,m}^{(A)\dagger}$ creates an electron on the A site of the unit cell at $\mathbf{R}_{nm} = na\hat{x} + mb\hat{y}$, where a and b are lattice spacings, and $n_{n,m}^{(\alpha)}$ is the number operator for sublattice $\alpha = $ A,B in the unit cell at $\mathbf{R}_{nm}$. Each unit cell contains one A site and one B site. The intra- and inter-unit-cell hopping strengths in the $\hat{x}$ direction are given by v and w, respectively, and the diagonal hopping strength is given by t_d. We include an on-site potential term for each sublattice, $\varepsilon^{A,B}$, and a chemical potential, μ. The first line of the above Hamiltonian corresponds to the standard 1D SSH model. These 1D SSH chains are coupled by the diagonal hopping included on the second line, which serves to extend the model to 2D. In all the results that follow, we take $v = 0.6$, $w = 1.2$, and $t_d = 0.9$. We provide an illustration of the lattice and hopping terms in Fig. 1.

The Hamiltonian in Eq. (1) can be viewed as a two-dimensional extension of the SSH Hamiltonian. We choose to present the model as a set of stacked SSH chains for the purposes of conceptualization, but such a model can arise in other quasi-2D materials as a result of structural distortions, for example a Peierls or Jahn-Teller distortion in one of the crystallographic directions, causing a transition from a tetragonal to an orthorhombic phase. In fact, such systems offer a better platform to realize the Weyl behavior discussed here because its presence requires the three hopping matrix elements v, w, and t_d to be of comparable magnitude.

In momentum space, the Hamiltonian can be written as

$$\mathcal{H}_0(\mathbf{k}) = -\mathbf{h}(\mathbf{k}) \cdot \boldsymbol{\sigma} + \bar{\varepsilon} - \mu, \tag{2}$$

where $\boldsymbol{\sigma} = (\sigma_x, \sigma_y, \sigma_z)$ is a vector of the Pauli matrices in the sublattice (pseudospin) basis, with $\bar{\varepsilon} = (\varepsilon^A + \varepsilon^B)/2$, and $\delta\varepsilon = (\varepsilon^B - \varepsilon^A)/2$. When $\varepsilon^A \neq \varepsilon^B$, inversion symmetry is broken. The vector $\mathbf{h}(\mathbf{k})$ has the form

$$\mathbf{h}(\mathbf{k}) = \begin{pmatrix} v_1 + w_1 \cos(k_x a) \\ w_1 \sin(k_x a) \\ \delta\varepsilon \end{pmatrix}, \tag{3}$$

with $v_1 = v + 2t_d \cos(k_y b)$ and $w_1 = w + 2t_d \cos(k_y b)$. This model has two pseudohelicity bands given by

$$E^\pm(\mathbf{k}) = \tilde{\mu} \pm |\mathbf{h}(\mathbf{k})|, \tag{4}$$

where $\tilde{\mu} = \bar{\varepsilon} - \mu$. The corresponding creation operators for states in these bands, $\chi_{\mathbf{k}}^{\dagger(\pm)}$, are related to the bare fermion operators according to

$$\begin{pmatrix} \chi_{\mathbf{k}}^{\dagger(-)} & \chi_{\mathbf{k}}^{\dagger(+)} \end{pmatrix} = \begin{pmatrix} c_{\mathbf{k}}^{\dagger(A)} & c_{\mathbf{k}}^{\dagger(B)} \end{pmatrix}$$

$$\times \frac{1}{\sqrt{2}} \begin{pmatrix} \sqrt{1 + \cos\theta_{\mathbf{k}}}\, e^{-i\phi_{\mathbf{k}}/2} & \sqrt{1 - \cos\theta_{\mathbf{k}}}\, e^{-i\phi_{\mathbf{k}}/2} \\ \sqrt{1 - \cos\theta_{\mathbf{k}}}\, e^{i\phi_{\mathbf{k}}/2} & -\sqrt{1 + \cos\theta_{\mathbf{k}}}\, e^{i\phi_{\mathbf{k}}/2} \end{pmatrix}, \tag{5}$$

where we have parametrized $\mathbf{h}(\mathbf{k})$ as $\mathbf{h}(\mathbf{k}) = |\mathbf{h}(\mathbf{k})|(\cos\phi_{\mathbf{k}} \sin\theta_{\mathbf{k}}, \sin\phi_{\mathbf{k}} \sin\theta_{\mathbf{k}}, \cos\theta_{\mathbf{k}})$, with $\phi_{\mathbf{k}} \equiv \tan^{-1}(\mathbf{h}_y/\mathbf{h}_x)$, and $\theta_{\mathbf{k}} \equiv \tan^{-1}(\sqrt{\mathbf{h}_x^2 + \mathbf{h}_y^2}/\mathbf{h}_z)$.

This band structure has two nodal points of opposite chirality, provided $\delta\varepsilon = 0$, whose locations are given by the solution of $E^+(\mathbf{k}) = E^-(\mathbf{k})$, which occurs at momenta $k_N^\pm = (0, \pm k_y^N)$, with $k_y^N = \cos^{-1}[-(v+w)/4t_d]$. Expanding $\mathbf{h}(\mathbf{k})$ in the vicinity of these nodal momenta (retaining only terms linear in $\mathbf{k}$), we obtain

$$\mathbf{h}_{\mathbf{k}}^{\text{linear}} = \begin{pmatrix} \pm 4t_d \sin(k_y^N)(k_y - k_y^N) \\ \frac{1}{2}(w - v)(k_x - k_x^N) \\ 0 \end{pmatrix}. \tag{6}$$

The linear behavior of the dispersion near these nodal points helps confirm their Weyl character. We note that while a finite $\delta\varepsilon$ opens a gap in the normal state, the addition of interactions

can lead to the realization of a Bogoliubov-Weyl semimetal characterized by the presence of nodal points, even when $\delta\varepsilon \neq 0$, as we will show later.

A topological characterization of this model can be found in Ref. [19], which also contains an investigation of the effects of an attractive Hubbard interaction using a combination of mean-field theory and auxiliary-field quantum Monte Carlo calculations. This study revealed that on-site interactions between like pseudospins lead to a superconducting phase with an intricate pairing structure, though the Fermi arcs that are present in the normal state do not persist in the superconducting state, which is topologically trivial.

As noted above, in the context of Weyl systems, it has been shown that topological superconducting states can emerge from conventional s-wave pairing interactions [34–36]. These models describe topological semimetals in the normal state, characterized by the presence of nodal points that carry topological charge. In the superconducting state, each node splits into a pair of Bogoliubov-Weyl nodes, and zero-energy Majorana states appear at the boundaries.

The model defined in Eq. (1) describes a topological semimetal in the normal state, when $\delta\varepsilon = 0$. Building on this model, we consider an interaction term that couples particles on opposite sublattices within the same unit cell. We observe that this interaction induces a topological superconducting state that supports both Bogoliubov-Weyl Fermi arcs and Majorana edge modes, without requiring more complicated momentum-dependent pairing terms, for instance of p-wave or d-wave form. Our observation of topological superconducting states in this model provides a simple description of the emergence of topological superconductivity from normal-state topological semimetals, and suggests that standard s-wave pairing interactions are sufficient to realize these states.

After adding this pairing term to our model, the total Hamiltonian can be written in the pseudospin basis as

$$
\hat{H} = \sum_{\mathbf{k}\alpha\beta} c_{\mathbf{k}}^{\dagger(\alpha)} \mathcal{H}_0(\mathbf{k})_{\alpha\beta} c_{\mathbf{k}}^{(\beta)}
$$
$$
+ \sum_{\mathbf{k}} \Delta^{\mathrm{AB}} c_{\mathbf{k}}^{\dagger(A)} c_{-\mathbf{k}}^{\dagger(B)} + \Delta^{\mathrm{BA}} c_{\mathbf{k}}^{\dagger(B)} c_{-\mathbf{k}}^{\dagger(A)} + \mathrm{H.c.}, \quad (7)
$$

where the pairing amplitude $\Delta^{\mathrm{AB}} = -\Delta^{\mathrm{BA}} \equiv \Delta_0$ is a momentum-independent constant.

We choose this pairing term based on its natural physical motivation. It is quite possible that this simple type of pairing interaction could arise in a quasi-2D system, such as the one described by our tight-binding Hamiltonian, given by Eq. (1), in its normal state. This Hamiltonian possesses a $(\pi, 0)$ charge-density-wave (CDW) order in the normal state. It has been well established in several quantum many-body systems [37–41], for instance, the cuprate superconductors [42,43], that the CDW order competes with the superconducting order. While these two types of order can coexist, in some cases partially or completely removing the CDW order opens up the superconductivity channel [44]. In our model, the onset of the CDW order is an indication of an effective attraction between fermions that leads to increased density along alternating bonds between the A and B sublattices.

It is reasonable to assume that this effective attraction will manifest itself in the superconducting channel if the CDW order is somehow suppressed, for instance by doping, which would likely lead to a pairing interaction between fermions on neighboring A and B atoms. This simple, though physically grounded picture suggests that the pairing term that we consider might be naturally realized in a wide class of quasi-2D materials.

In the pseudohelicity basis, the Hamiltonian in Eq. (7) can be written as

$$
\hat{H} = \sum_{\mathbf{k},\alpha=\pm} E^\alpha(\mathbf{k}) \chi_{\mathbf{k}}^{\dagger(\alpha)} \chi_{\mathbf{k}}^{(\alpha)} + \sum_{\mathbf{k},\rho\tau} \tilde{\Delta}_{\rho\tau}(\mathbf{k}) \chi_{\mathbf{k}}^{\dagger(\rho)} \chi_{-\mathbf{k}}^{\dagger(\tau)} + \mathrm{H.c.},
$$
$$(8)$$

where $E^\pm(\mathbf{k})$ is defined in Eq. (4), $\tilde{\Delta}_{--}(\mathbf{k}) = -\tilde{\Delta}_{++}(\mathbf{k}) = i \sin\theta_{\mathbf{k}} \sin\phi_{\mathbf{k}}$, and $\tilde{\Delta}_{-+}(\mathbf{k}) = -\tilde{\Delta}_{+-}^*(\mathbf{k}) = -(\cos\phi_{\mathbf{k}} + i \sin\phi_{\mathbf{k}} \cos\theta_{\mathbf{k}})$.

We note that the gap matrix $\tilde{\Delta}_{\rho\tau}(\mathbf{k})$ is momentum dependent, with momentum-space behavior closely connected to the topological character of the noninteracting band structure. Making use of Eq. (6), we find that in the vicinity of the nodal points, the gap function $\tilde{\Delta}_{-+}(\mathbf{k}) \propto \alpha(k_y - k_y^N) + i\beta(k_x - k_x^N)$, and $\tilde{\Delta}_{--}(\mathbf{k}) = -\tilde{\Delta}_{++}(\mathbf{k}) \propto i\gamma(k_x - k_x^N)$ where α, β, and γ are real coefficients. This p-wave structure naturally emerges from the simple momentum-independent pairing term that we have introduced into the model. The appearance of this phase in the gap function can be understood as a consequence of the fact that spinless fermions cannot pair on-site due to the Pauli exclusion principle. However, because this is the same phase that parametrizes the normal-state band structure and wave functions, the topological character of the phase in the gap function is acquired from the normal state. In other words, the phase of the gap function is nontrivial because it is the same phase that generates the topological features of the normal-state band structure. This is a similar observation to previous studies on pairing in spinless models that possess topological band structures in the normal state [45,46], though unlike these studies, our lattice model preserves time-reversal symmetry.

The full Hamiltonian can be diagonalized exactly, yielding eigenvalues,

$$
E_\pm^1(\mathbf{k}) = \pm\sqrt{\eta^2 + 2|\zeta|},
$$
$$
E_\pm^2(\mathbf{k}) = \pm\sqrt{\eta^2 - 2|\zeta|}, \quad (9)
$$

where we have defined

$$
\eta^2 = \tilde{\mu}^2 + \delta\varepsilon^2 + |h_{\mathbf{k}}|^2 + |\Delta|^2, \quad (10)
$$

$$
\zeta^2 = (|h_{\mathbf{k}}|^2 + \delta\varepsilon^2)\tilde{\mu}^2 + (h_{\mathbf{k}}^{x\,2} + \delta\varepsilon^2)|\Delta|^2. \quad (11)
$$

Band degeneracies occur where $E_+^2(\mathbf{k}) = E_-^2(\mathbf{k}) = 0$. This leads to the condition

$$
\eta^2 = 2|\zeta|, \quad (12)
$$

which has four solutions at $k_x = 0$,

$$
\pm k_y^{N,\pm} = \cos^{-1}\left[\frac{\pm\sqrt{\tilde{\mu}^2 - \delta\varepsilon^2 + |\Delta|^2} - (v+w)}{4t_d} \right]. \quad (13)
$$
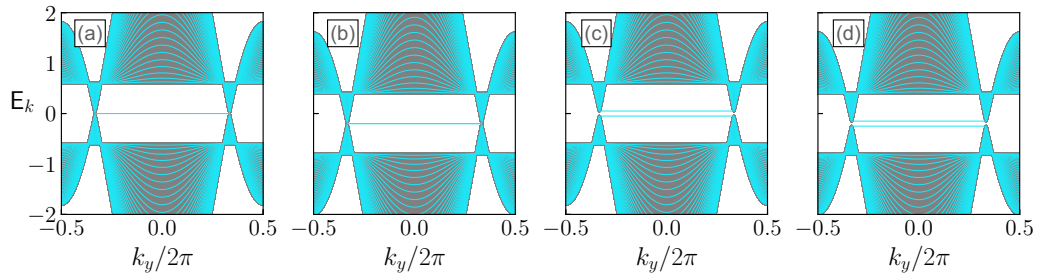
FIG. 2. Edge spectrum for a noninteracting system. The color curves show the results from a slab calculation, while the bulk is shown in gray. From left to right, $(\mu, \delta\varepsilon) = (0, 0), (0.2, 0), (0, 0.1), (0.2, 0.1)$.

These correspond to the two original nodal points at $\{0, \pm\cos^{-1}[-(v + w)/4t_d]\}$, which are now split into four nodal points, with the pairs of nodes centered on $\{0, \pm\cos^{-1}[-(v + w)/4t_d]\}$, but shifted by the finite $\tilde{\mu}$, $\delta\varepsilon$, and Δ. In the case of $\tilde{\mu} = \delta\varepsilon = \Delta = 0$, we recover the noninteracting result. We note that while the noninteracting spectrum is gapped for $\delta\varepsilon \neq 0$, this gap can be closed with the addition of a pairing interaction.

The solutions identified above exist across a large region of the parameter space. However, limiting ourselves to the case of $\delta\varepsilon = 0$, an additional set of solutions exists when the following relation is satisfied:

$$\mu^2 + |\Delta|^2 = (v - w)^2. \tag{14}$$

This results in a set of nodal lines, with one along the k_y direction at $k_x = \pi$, and another two in the k_x direction at $k_y = \pm\cos^{-1}(-w/2t_d)$.

III. TOPOLOGICAL SUPERCONDUCTIVITY

The analysis above shows that the addition of a pairing term coupling fermions on different sublattices within the same unit cell leads to the splitting of each original nodal point into a pair of Bogoliubov-Weyl nodes. In order to characterize the topological nature of this state, we proceed by computing the edge spectrum and the Berry connection vector, which provide clear evidence of Majorana modes and a topological transition as a function of the pairing strength, Δ_0, and the chemical potential, μ.

A. Edge spectrum and Majorana states

To obtain the edge spectrum for the system, we diagonalize the Hamiltonian in a slab geometry (with finite x dimension).

The edge spectrum reveals the presence of both Majorana states at zero energy and Fermi arc states. We first present an example of the edge spectrum for the noninteracting model. The noninteracting system remains gapless for finite chemical potential [Fig. 2(b)], which simply shifts the Fermi level. With finite $\delta\varepsilon$, a gap opens, separating the pair of Fermi arc states [Fig. 2(c)]. When μ and $\delta\varepsilon$ are both finite, the Fermi level shifts and a gap opens [Fig. 2(d)].

In the interacting system, the pair of Weyl nodes is split into two pairs of Bogoliubov-Weyl nodes. There are four Fermi arc states passing through the origin that connect the inner nodes. These four states are degenerate at $\mu = \delta\varepsilon = 0$ [Fig. 3(a)]. The degeneracy is partially lifted by finite μ [Fig. 3(b)], which splits the states into two pairs related by particle-hole symmetry and also by finite $\delta\varepsilon$ [Fig. 3(c)]. With finite μ and finite $\delta\varepsilon$, the degeneracy is fully lifted [Fig. 3(d)]. In addition to the Fermi arc states, there is a pair of Majorana states at zero energy connecting the inner node near k_N^+ to the outer node near k_N^+, and similarly for the pair of nodes around k_N^-.

In order to characterize the topological nature of the edge states, we examine the components of their wave functions. Majorana states are defined by the property of their creation and annihilation operators, $\gamma_{\mathbf{k}}^{\dagger} = \gamma_{-\mathbf{k}}$. For the case of finite x dimension, the Hamiltonian can be diagonalized by Bogoliubov operators of the general form

$$\gamma_{k_y}^{n\dagger} = \sum_i a_{i,k_y}^n \chi_{i,k_y}^{\dagger(+)} + b_{i,k_y}^n \chi_{i,k_y}^{\dagger(-)} + c_{i,k_y}^n \chi_{i,-k_y}^{(+)} + d_{i,k_y}^n \chi_{i,-k_y}^{(-)},$$

$$\tag{15}$$

where n labels the eigenstate and i labels the layer in the finite direction. The Majorana condition $\gamma_{\mathbf{k}}^{\dagger} = \gamma_{-\mathbf{k}}$, leads to

FIG. 3. Edge spectrum for an interacting system with $\Delta_0 = 0.3$. From left to right, $(\mu, \delta\varepsilon) = (0, 0), (0.2, 0), (0, 0.1), (0.2, 0.1)$.
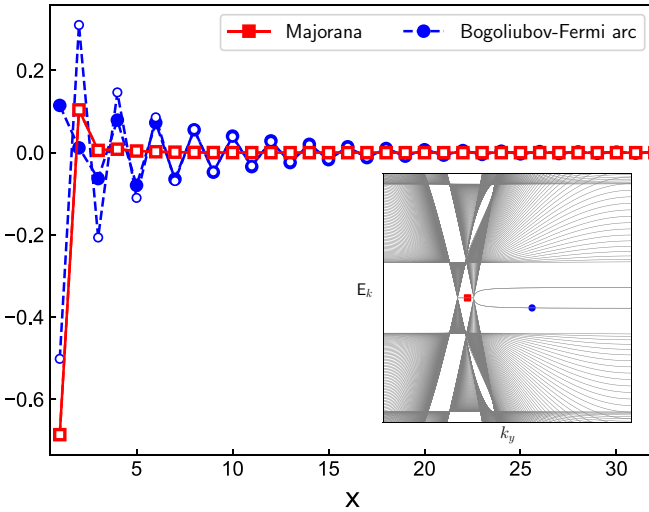
FIG. 4. Wave-function amplitudes vs x. We plot the components a_{i,k_y} (filled symbols) and $(c_{i,-k_y})^*$ (empty symbols) of the eigenvectors for a Majorana state and a Bogoliubov-Fermi arc state. Per the condition in Eq. (17), we classify the state with $a_{i,k_y} = (c_{i,-k_y})^*$ as a Majorana state and the state with $a_{i,k_y} \neq (c_{i,-k_y})^*$ as a Bogoliubov-Fermi arc state. The inset shows the edge spectrum, with the symbols indicating the momentum corresponding to the Majorana (red square) and Bogoliubov-Fermi arc (blue circle) states shown in the main panel. We take $\Delta_0 = 0.3$ and $\mu = 0.1$.

the requirement (dropping the label n)

$$\sum_i a_{i,k_y} \chi_{i,k_y}^{\dagger(+)} + b_{i,k_y} \chi_{i,k_y}^{\dagger(-)} + c_{i,k_y} \chi_{i,-k_y}^{(+)} + d_{i,k_y} \chi_{i,-k_y}^{(-)}$$

$$= \sum_j (a_{j,-k_y})^* \chi_{j,-k_y}^{(+)} + (b_{j,-k_y})^* \chi_{j,-k_y}^{(-)} + (c_{j,-k_y})^* \chi_{j,k_y}^{\dagger(+)}$$

$$+ (d_{j,-k_y})^* \chi_{j,k_y}^{\dagger(-)}, \tag{16}$$

which implies, for a Majorana state (up to an arbitrary phase),

$$a_{i,k_y} = (c_{i,-k_y})^*, \quad b_{i,k_y} = (d_{i,-k_y})^*,$$

$$c_{i,k_y} = (a_{i,-k_y})^*, \quad d_{i,k_y} = (b_{i,-k_y})^*. \tag{17}$$

In Fig. 4, we plot the amplitudes a_{i,k_y} and $(c_{i,-k_y})^*$ of the wave function for two states, both of which are localized on the edge of the system. We identify one state as Majorana due to the relationship between its amplitudes, as described above (though not shown, the remaining coefficients satisfy the same condition). The other state shown is a Bogoliubov-Fermi arc state, which lies in the bulk gap but is not pinned to zero energy at finite chemical potential and does not satisfy the Majorana condition.

B. Topological transition

Having confirmed the topological nature of the superconducting state that emerges in the interacting model, which is characterized by the presence of Majorana states in the edge spectrum, we now study the effect of chemical potential and pairing strength on this state. As we describe in the following, we observe a topological transition as a function of pairing strength and chemical potential, marked by a qualitative change in the edge spectrum and the behavior of the Berry connection vector. We note that we have also computed the Berry phase around each node, which is a gauge-independent quantity, to verify our conclusions.

In Fig. 5, we examine the edge spectrum and Berry connection vector versus Δ at fixed chemical potential. The Berry connection vector is calculated as $\mathbf{A} \equiv -i \langle \psi^- | \nabla_{\mathbf{k}} | \psi^- \rangle$, where $|\psi^-\rangle = (u_{\mathbf{k}}^1, u_{\mathbf{k}}^2, u_{\mathbf{k}}^3, u_{\mathbf{k}}^4)^\mathsf{T}$ is the wave function corresponding to the lower Bogoliubov-Weyl band, with complex coefficients $u_{\mathbf{k}}^i$. This yields

$$\mathbf{A} = \frac{1}{2} \sum_i |u_{\mathbf{k}}^i|^2 \nabla_{\mathbf{k}} \varphi_{\mathbf{k}}^i, \tag{18}$$

where $\varphi_{\mathbf{k}}^i$ is the phase of the complex coefficient $u_{\mathbf{k}}^i$.
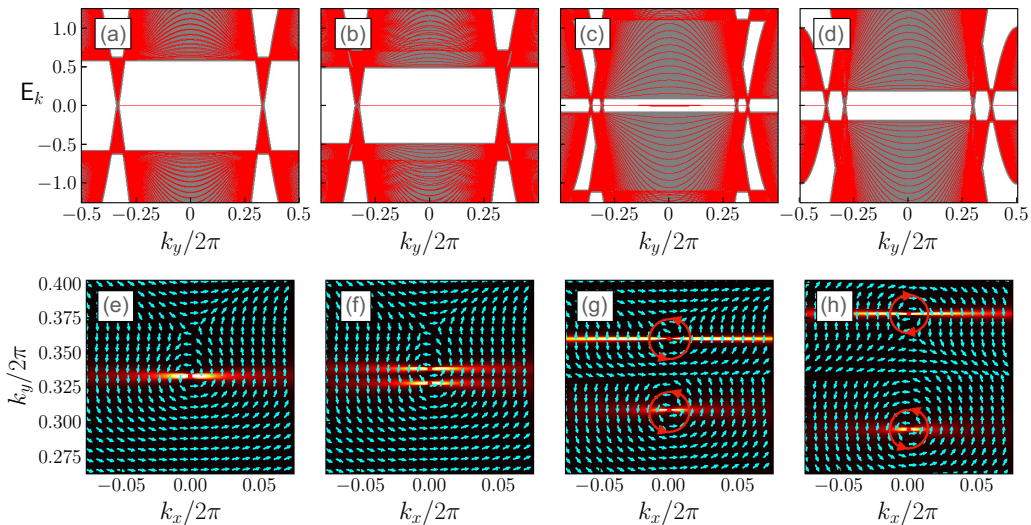
FIG. 5. Edge spectrum and Berry connection vector vs Δ at $\mu = 0.0$. (a), (e) $\Delta = 0.01$, (b), (f) $\Delta = 0.1$, (c), (g) $\Delta = 0.5$, (d), (h) $\Delta = 0.8$. The top row shows the edge spectrum (red curves); the bulk region is shown in gray. The bottom row shows the Berry connection vector around the pair of nodes in the upper BZ, with the direction given by the cyan arrows and the magnitude given by the color density plot. The red circles with arrows are a guide to the eye showing the circulation pattern of the Berry connection vector around either node (indicated by the small red dot) in the upper half of the BZ, before and after the transition.
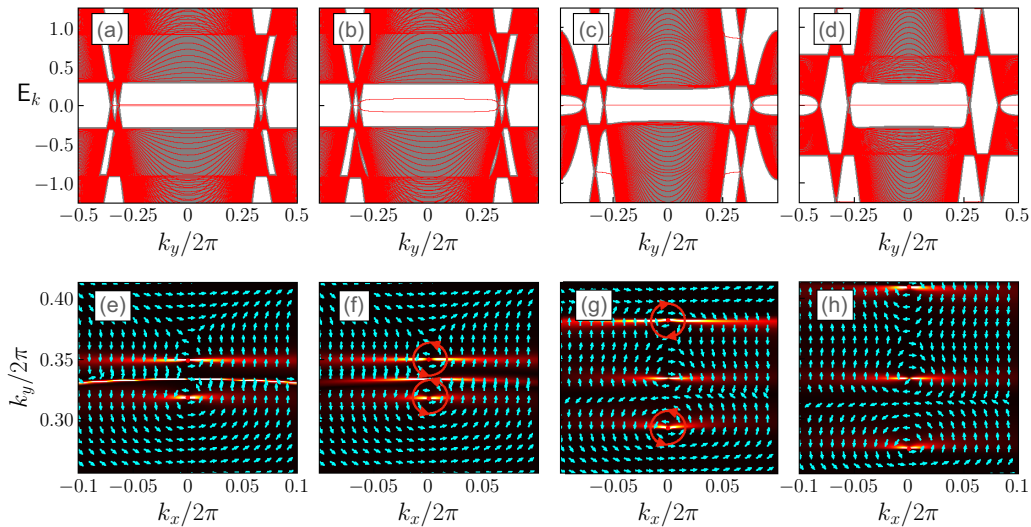
FIG. 6. Edge spectrum and Berry connection vector vs μ at $\Delta = 0.3$. (a), (e) $\mu = 0.01$, (b), (f) $\mu = 0.1$, (c), (g) $\mu = 0.8$, (d), (h) $\mu = 1.2$. The top row shows the edge spectrum (red curves); the bulk region is shown in gray. The bottom row shows the Berry connection vector around the pair of nodes in the upper BZ, with the direction given by the cyan arrows and the magnitude given by the color density plot. The red circles with arrows are a guide to the eye showing the circulation pattern of the Berry connection vector around either node (indicated by the small red dot) in the upper half of the BZ, before and after the transition.

In the limit of $\Delta \to 0$ [Figs. 5(a) and 5(e)], the edge spectrum and the Berry connection vector resemble those of the noninteracting model, which is characterized by a Fermi arc state connecting nodes of opposite chirality. As described above, at finite Δ, each of the original nodal points splits into a pair of Bogoliubov-Weyl nodes. At small Δ, Figs. 5(b), 5(f) and 5(c), 5(g), there are four Bogoliubov-Weyl Fermi arc states connecting the nodes closest to the origin. These states are degenerate at $\mu = \delta\varepsilon = 0$.

With increasing Δ, at a fixed value of chemical potential, each pair of Bogoliubov-Weyl nodes begins to separate and the Berry connection begins to deviate from the noninteracting result. Further increasing Δ leads to the emergence of four distinct sources of topological charge (two in each half of the Brillouin zone), as indicated by the Berry connection vector.

Below a critical value of $\Delta = \Delta_c$, given by Eq. (14), these charges are of the same sign on a given half of the Brillouin zone (BZ), as indicated by the direction of circulation of the Berry connection vector around the node [Figs. 5(c) and 5(g)]. Above Δ_c, we observe a transition to a state with topological charges of opposite sign on the same half of the Brillouin zone [Figs. 5(d) and 5(h)], indicated by the opposite direction of circulation of the Berry connection around either node on the same half of the Brillouin zone.

This transition is also reflected in the edge spectrum. At small to intermediate Δ, below the critical value, we find a pair of Majorana states connecting each pair of Bogoliubov-Weyl nodes, in addition to four Bogoliubov-Weyl Fermi arc states connecting the nodes closer to the origin of the Brillouin zone. Past Δ_c, the system again has four Bogoliubov-Weyl nodes, but now four Majorana states. These two nodal semimetallic states are connected by a nodal-line semimetallic state, which occurs at Δ_c, given by the solution of Eq. (14). We observe a similar transition as a function of increasing μ for a fixed value of Δ (Fig. 6).

IV. CONCLUSION

In this work, we have constructed a lattice model that extends the well-known SSH model into two dimensions. In the absence of interactions, the model hosts a pair of Weyl nodes in its band structure. The addition of a momentum-independent pairing interaction coupling fermions on different sublattices within the same unit cell splits each node into a pair of Bogoliubov-Weyl nodes and induces a topological superconducting state, characterized by a pairing function with a nontrivial phase whose origin is connected to the topological band structure of the normal state. The topological superconductor state supports both Majorana and Fermi arc states, whose number and orientation are sensitive to the pairing strength and chemical potential, which induce a topological transition marked by the closing and reopening of the bulk gap accompanied by a qualitative change in the edge spectrum.

Given the potential applications of topological superconductors, for instance in the field of quantum computing and information, a more complete understanding of the origins of these states remains an important goal. Here we have presented a simple model with a physically motivated pairing interaction that serves as a clear illustration of the emergence of a topological superconducting state from a Weyl semimetal system. This description helps shed light on the connection between topological superconductivity and topological band structures and suggests compelling new avenues in the search for material realizations of topological superconductivity.

[1] M. Z. Hasan and C. L. Kane, Rev. Mod. Phys. **82**, 3045 (2010).

[2] B. A. Bernevig and T. L. Hughes, *Topological Insulators and Topological Superconductors* (Princeton University Press, Princeton, 2013).

[3] W. P. Su, J. R. Schrieffer, and A. J. Heeger, Phys. Rev. Lett. **42**, 1698 (1979).

[4] M. J. Rice and E. J. Mele, Phys. Rev. Lett. **49**, 1455 (1982).

[5] J. Zak, Phys. Rev. Lett. **62**, 2747 (1989).

[6] A. J. Heeger, S. Kivelson, J. R. Schrieffer, and W. P. Su, Rev. Mod. Phys. **60**, 781 (1988).

[7] M. Atala, M. Aidelsburger, J. T. Barreiro, D. Abanin, T. Kitagawa, E. Demler, and I. Bloch, Nat. Phys. **9**, 795 (2013).

[8] D. J. Thouless, Phys. Rev. B **27**, 6083 (1983).

[9] L. Wang, M. Troyer, and X. Dai, Phys. Rev. Lett. **111**, 026802 (2013).

[10] S. Nakajima, T. Tomita, S. Taie, T. Ichinose, H. Ozawa, L. Wang, M. Troyer, and Y. Takahashi, Nat. Phys. **12**, 296 (2016).

[11] M. Lohse, C. Schweizer, O. Zilberberg, M. Aidelsburger, and I. Bloch, Nat. Phys. **12**, 350 (2016).

[12] M. Leder, C. Grossert, L. Sitta, M. Genske, A. Rosch, and M. Weitz, Nat. Commun. **7**, 13112 (2016).

[13] F. A. An, E. J. Meier, and B. Gadway, Phys. Rev. X **8**, 031045 (2018).

[14] B. Pérez-González, M. Bello, A. Gómez-León, and G. Platero, Phys. Rev. B **99**, 035146 (2019).

[15] L. Li, Z. Xu, and S. Chen, Phys. Rev. B **89**, 085111 (2014).

[16] N. Sun and L.-K. Lim, Phys. Rev. B **96**, 035139 (2017).

[17] J. Jünemann, A. Piga, S.-J. Ran, M. Lewenstein, M. Rizzi, and A. Bermudez, Phys. Rev. X **7**, 031057 (2017).

[18] P. M. Tam, J. W. F. Venderbos, and C. L. Kane, Phys. Rev. B **105**, 045106 (2022).

[19] P. Rosenberg, N. Aryal, and E. Manousakis, Phys. Rev. B **100**, 104522 (2019).

[20] P. Rosenberg and E. Manousakis, Phys. Rev. B **104**, 134511 (2021).

[21] H. Leng, C. Paulsen, Y. K. Huang, and A. de Visser, Phys. Rev. B **96**, 220506(R) (2017).

[22] Z. Guguchia, F. von Rohr, Z. Shermadini, A. T. Lee, S. Banerjee, A. R. Wieteska, C. A. Marianetti, B. A. Frandsen, H. Luetkens, Z. Gong, S. C. Cheung, C. Baines, A. Shengelaya, G. Taniashvili, A. N. Pasupathy, E. Morenzoni, S. J. L. Billinge, A. Amato, R. J. Cava, R. Khasanov *et al.*, Nat. Commun. **8**, 1082 (2017).

[23] D. Rhodes, R. Schönemann, N. Aryal, Q. Zhou, Q. R. Zhang, E. Kampert, Y.-C. Chiu, Y. Lai, Y. Shimura, G. T. McCandless, J. Y. Chan, D. W. Paley, J. Lee, A. D. Finke, J. P. C. Ruff, S. Das, E. Manousakis, and L. Balicas, Phys. Rev. B **96**, 165134 (2017).

[24] D. A. Rhodes, A. Jindal, N. F. Q. Yuan, Y. Jung, A. Antony, H. Wang, B. Kim, Y.-c. Chiu, T. Taniguchi, K. Watanabe, K. Barmak, L. Balicas, C. R. Dean, X. Qian, L. Fu, A. N. Pasupathy, and J. Hone, Nano Lett. **21**, 2505 (2021).

[25] D. A. Ivanov, Phys. Rev. Lett. **86**, 268 (2001).

[26] A. Kitaev, Ann. Phys. **303**, 2 (2003).

[27] J. Alicea, Rep. Prog. Phys. **75**, 076501 (2012).

[28] D. Aasen, M. Hell, R. V. Mishmash, A. Higginbotham, J. Danon, M. Leijnse, T. S. Jespersen, J. A. Folk, C. M. Marcus, K. Flensberg, and J. Alicea, Phys. Rev. X **6**, 031016 (2016).

[29] T. Karzig, C. Knapp, R. M. Lutchyn, P. Bonderson, M. B. Hastings, C. Nayak, J. Alicea, K. Flensberg, S. Plugge, Y. Oreg, C. M. Marcus, and M. H. Freedman, Phys. Rev. B **95**, 235305 (2017).

[30] N. Read and D. Green, Phys. Rev. B **61**, 10267 (2000).

[31] Y. Ueno, A. Yamakage, Y. Tanaka, and M. Sato, Phys. Rev. Lett. **111**, 087002 (2013).

[32] C. Nayak, S. H. Simon, A. Stern, M. Freedman, and S. Das Sarma, Rev. Mod. Phys. **80**, 1083 (2008).

[33] C. Zhang, S. Tewari, R. M. Lutchyn, and S. Das Sarma, Phys. Rev. Lett. **101**, 160401 (2008).

[34] T. Meng and L. Balents, Phys. Rev. B **86**, 054504 (2012).

[35] G. Bednik, A. A. Zyuzin, and A. A. Burkov, Phys. Rev. B **92**, 035153 (2015).

[36] Z. Faraei and S. A. Jafari, Phys. Rev. B **100**, 035447 (2019).

[37] R. T. Scalettar, N. E. Bickers, and D. J. Scalapino, Phys. Rev. B **40**, 197 (1989).

[38] F. C. Zhang, M. Ogata, and T. M. Rice, Phys. Rev. Lett. **67**, 3452 (1991).

[39] R. M. Noack, D. J. Scalapino, and R. T. Scalettar, Phys. Rev. Lett. **66**, 778 (1991).

[40] B.-X. Zheng, C.-M. Chung, P. Corboz, G. Ehlers, M.-P. Qin, R. M. Noack, H. Shi, S. R. White, S. Zhang, and G. K.-L. Chan, Science **358**, 1155 (2017).

[41] F. H. Yu, D. H. Ma, W. Z. Zhuo, S. Q. Liu, X. K. Wen, B. Lei, J. J. Ying, and X. H. Chen, Nat. Commun. **12**, 3645 (2021).

[42] J. Chang, E. Blackburn, A. T. Holmes, N. B. Christensen, J. Larsen, J. Mesot, R. Liang, D. A. Bonn, W. N. Hardy, A. Watenphul, M. v. Zimmermann, E. M. Forgan, and S. M. Hayden, Nat. Phys. **8**, 871 (2012).

[43] E. Fradkin, S. A. Kivelson, and J. M. Tranquada, Rev. Mod. Phys. **87**, 457 (2015).

[44] Z.-X. Li, M. L. Cohen, and D.-H. Lee, Phys. Rev. B **100**, 245105 (2019).

[45] S. Murakami and N. Nagaosa, Phys. Rev. Lett. **90**, 057002 (2003).

[46] Y. Li and F. D. M. Haldane, Phys. Rev. Lett. **120**, 067003 (2018).